Electronic Supplementary Material (ESI) for Nanoscale.

Supporting Information

Controllable Design of Defect-Rich Hybrid Fe_xO_y Nanostructures on Mesoporous Carbon-based Scaffold for Pseudocapacitive Applications

Sajjad S. Mofarah,*[a] Rasoul Khayyam Nekouei,[a] Samane Maroufi,[a] Smitirupa Biswal,[a] Sean Lim,[b] Yin Yao,[b] and Veena Sahajwalla[a]

[a] Centre for Sustainable Materials Research and Technology, SMaRT@UNSW School of Materials Science and Engineering UNSW Sydney, NSW 2052, Australia

[b] Electron Microscopy Unit (EMU)Mark Wainwright Analytical Centre UNSW Sydney, NSW 2052, Australia

Materials and Methods

Table S1. Chemical analysis of fresh and transformed coffee precursors.

Sample	Coffee	Transformed coffee
Composition	Weight (%)	Weight (%)
Ash	2.6	10.5
Volatile	79.5	20.4
Fixed Carbon	16.7	63.4
Total Carbon	51.6	65.9
Hydrogen	6.24	2.44
Sulphur	0.16	0.27
Nitrogen	2.43	4.48
Oxygen	35.77	10.71

Table S2. Ash compositions of transformed coffee via X-ray fluorescence (XRF) analysis.

Metal oxides	SiO_2	Al_2O_3	Fe_2O_3	Mn_3O_4	MgO	CaO	Na_2O	K_2O	P_2O_5	SO_3
(weight %)	0.70	0.31	0.31	0.28	18.30	11.95	3.56	29.35	17.23	5.49

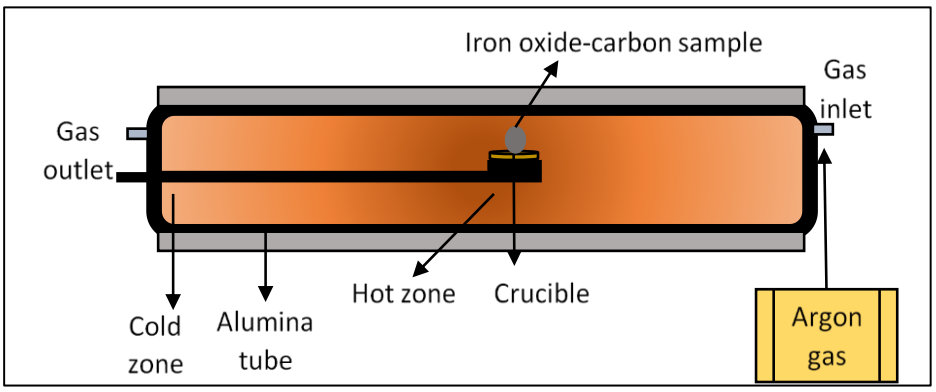

Fig. S1. Schematic of heat treatment setup.

- The heating rate of the tube furnace is 100˚C·h^{-1}, so programming of the furnace to the requisite temperature (950, 850, and 750) is done accordingly.
- After the required temperature is attained, the crucible containing the sample is initially placed in the cold zone (which is usually at a temperature of 150-250˚C) for 10 min and then pushed into the hot zone (it is at the temperature we want to operate) to avoid any thermal shock.
- The dwelling time in the hot zone is 10 min under an argon gas atmosphere with a flow rate of 1 L/min.
- After residing in the hot zone, the sample is pulled back into the cold zone and then kept there for another 10 min before being taken out of the furnace. The approximate cooling rate is 30-50˚C·s^{-1}
- Initial sample mix consists of iron oxide and carbon mixed with an iron oxide/carbon molar ratio of 1:3. Experiments were performed by taking required amount from the following mixture:

Table S3. Mass analysis of hybrid Fe_xO_y before and after heat treatment.

Sample mix and temperature	Initial weight (g)	Final weight (g)
Sample with TC -950	0.3324	0.2281
Sample with TC-850	0.3812	0.3380
Sample with TC-750	0.3068	0.2772

Materials and Methods for Pseudocapacitance application tests:

A potentiostat/galvanostat (VSP-300 BioLogic) equipped with EIS was employed for electrochemical analysis in energy storage application. A conventional three-electrode configuration system was employed, in which standard calomel electrode (SCE) and spiral Pt wire were applied as reference and auxiliary electrodes, respectively. A glassy carbon electrode with a diameter of 3 mm, ~7 mm^2, was used as the substrate of working electrode. Then, the prepared inked, including active material, superconductive carbon (Super P Carbon from Sigma Aldrich), deionised (DI) water, and Isopropanol, was drop-casted on the surface of the glassy carbon. The ingredients of inks were agitated and mixed thoroughly by sonication and mechanical vortex mixing. After drying, the electrode was applied in a 5M KOH solution for electrochemical benchmarking.

Table S4. Details for preparation process of electrodes for supercapacitance applications.

No.	Samples	DI Water (µL)	Isopropanol (µL)	Nafion 5% (µL)	Carbon (mg)	Active material (mg)
1st series						
1	C super conductive (P)	150	150	10	5.6	-
2	Carbon Black (CB)	150	150	10	5.5	-
3	750	150	150	10	-	5.8
4	850	150	150	10	-	6.2
5	950	150	150	10	-	5.6
6	TC	150	150	10	-	6.0
2nd series						
9	850	300	300	20	2.3 (P)	8.0
10	750	300	300	20	2.3 (P)	7.7
11	TC	300	300	20	2.4 (P)	7.8
12	950	300	300	20	2.3 (P)	8.0
13	α-Fe_2O_3	300	300	20	2.5 (P)	8.1
14	Fresh coffee	300	300	20	2.6 (P)	8.0

Characterisation

Scanning electron microscopy (SEM)

Scanning electron microscopy images were obtained by SEM (FEI Nova NanoSEM; secondary electron emission; accelerating voltage 5 kV, Hillsboro, OR, USA).

Transmission electron microscopy (TEM)

The Fe_xO_y nanoparticles were suspended in water and drop-casted onto a carbon-supported Cu grid followed by air-drying at room temperature. The prepared samples were used for TEM and energy dispersive spectroscopy (EDS). High-resolution transmission TEM (HRTEM) images and EDS analysis of the nanostructures were taken by a Philips CM 200 microscope (Eindhoven, the Netherlands). Data analysis including construction of FFT patterns and measurement of d-spacing were conducted using Gatan (GMS 3) software.

X-ray diffraction (XRD)

Mineralogical data for the nanostructures were obtained using a Philips X'Pert Multipurpose X-ray diffractometer (Almelo, Netherlands) with CoK_α radiation, 40 kV, 20 mA, scan range 10°-80° 2θ, and scan speed 0.2 2θ.min^{-1}. Further, the *in-situ*, high-temperature XRD analysis was done using a Philips X'Pert Multipurpose X-ray diffractometer (Almelo, Netherlands) with CuK_α radiation, 40 kV, 20 mA, scan range 20°-90° 2θ, and scan speed 0.2 2θ.min^{-1}. The temperature was set to 950°C with the heating rate of 2 °C.min^{-1}. The sample was placed on a Pt plate under N_2 atmosphere to avoid reactions in elevating temperatures. The peaks were analysed using X'Pert High Score Plus software (Malvern, UK).

Laser Raman microspectroscopy (Raman)

Raman test was carried out using a Renishaw inVia confocal Raman microscope (Gloucestershire, UK) equipped with a helium-neon green laser (514 nm) and grating of 1800 g mm^{-1}. The Raman results were obtained at laser power of 35 mW, spot size of ~1 µm, and applied 0.01% laser power. Raman analysis was conducted using Renishaw WiRE 4.4 software.

Photoluminescence (PL)

The PL spectroscopy was carried out using a spectrofluorophotometer (RF-5301PC, Shimadzu, Kyoto, Japan). The results were obtained at laser (514 nm) with the spot size of ~ 1 µm. The results were analysed using Renishaw WiRE 4.4 and OriginLab software.

X-ray photoelectron spectroscopy (XPS)

The surface chemical characterisation of the samples was investigated using a Thermo Fisher Scientific ESCALAB 250Xi spectrometer (Loughborough, Leicestershire, UK) equipped with a monochromatic Al Kα source (1486.6 eV) hemispherical analyser. The chamber pressure during the analysis was kept constant at <8-10 mbar. The acquired binding energies were referenced to the C1s signal corrected to 285 eV and the spectra were fitted using a convolution of Lorentzian and Gaussian profiles.

Electron Paramagnetic Resonance (EPR)

EPR analysis was conducted using a Bruker EMX X-Band ESR Spectrometer with constant frequency at 9.8 GHz. The EPR data were recorded over the centre Field at 3200 mT, modulation amplitude at 4 G, and microwave power at 0.6325 mW. The processing on EPR spectra was carried out using Bruker Xenon software.

Additional characterisation and analysis

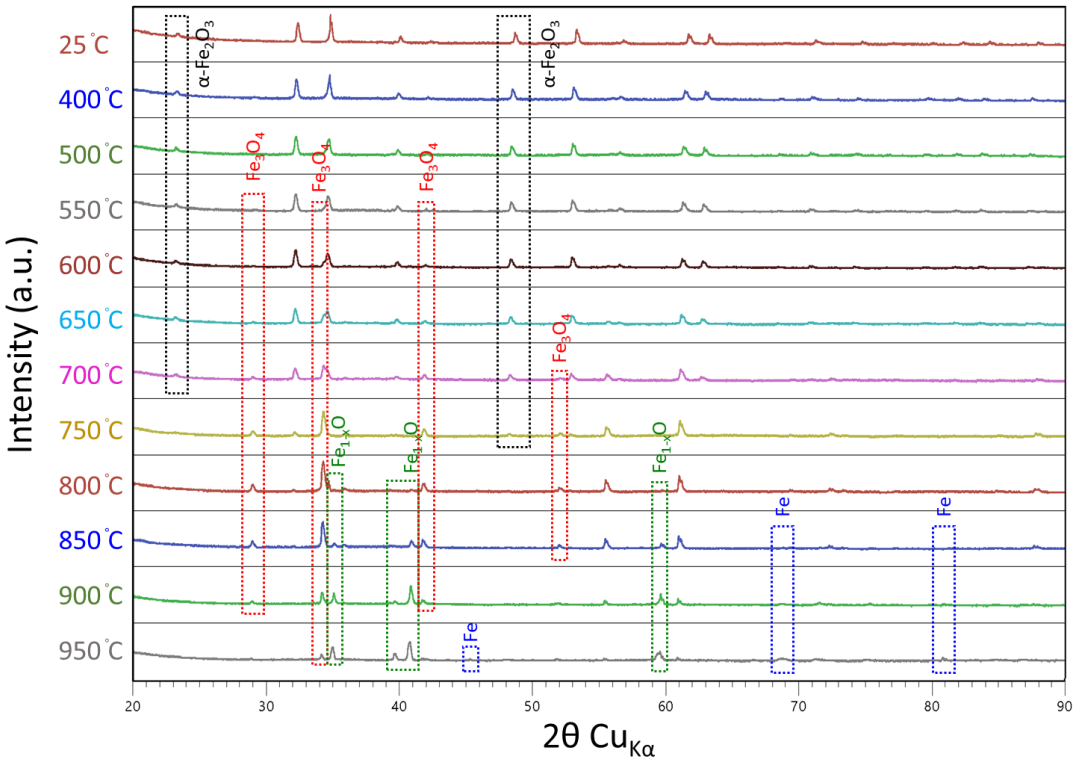

Fig. S2 *in-situ* XRD patterns of α-Fe_2O_3 during heating to 950 ˚C in the presence of transformed carbon.

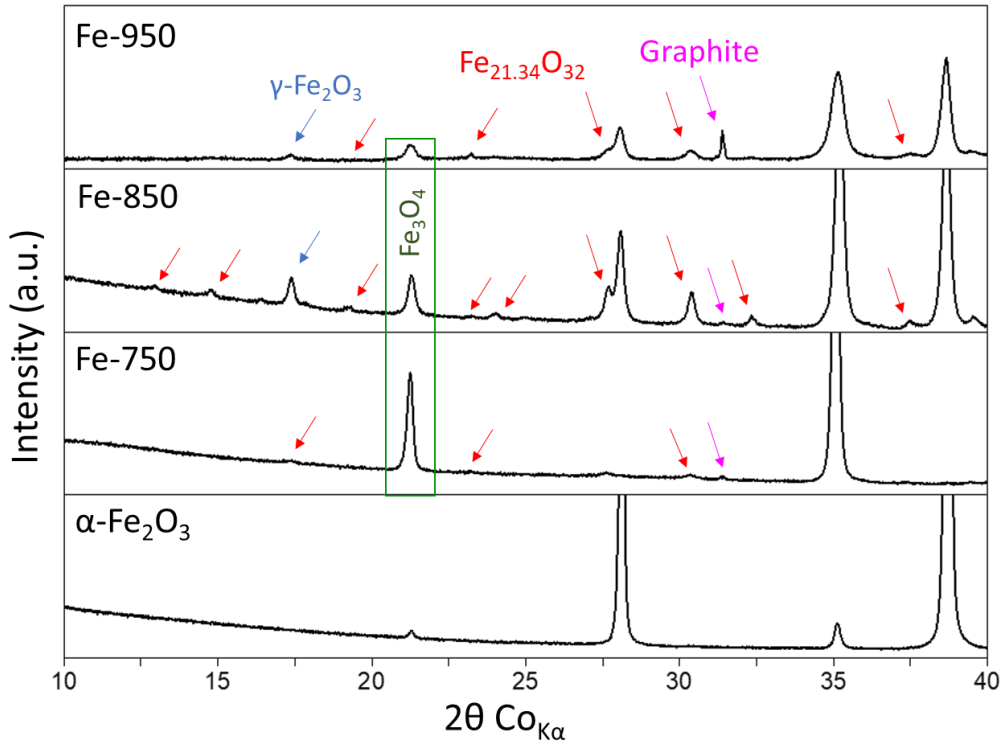

Fig. S3 XRD patterns of α-Fe_2O_3, Fe-750, Fe-850, and Fe-950 at 2θ = 10-40°. The peaks pointed by red arrows are ascribed to non-stoichiometric $Fe_{21.34}O_{32}$ and the peak pointed by blue arrow is attributed to graphite structure.

FTIR analysis: Fig. S4 shows the results of Fourier transform infrared spectroscopy (FTIR) analysis for fresh and transformed coffee. As for the fresh coffee (FC), the asymmetrically broad peak at wavenumber ~ 3000 cm^{-1} is attributed to the stretching vibrational mode of hydroxyl (OH) group or physically adsorbed H_2O molecules in the fresh coffee. The two sharp bands positioned at ~2900 and ~2850 cm^{-1} associates with the asymmetric stretching vibrational modes of C-H bonds. Additionally, there are two peaks at 1700 cm^{-1} and ~1600 cm^{-1}. The former is attributed to the C=O bonds of ester functional groups in chlorogenic acids and caffeine, while the latter is related to the C=C bond of aromatic groups in the lignin components. More importantly, the predominant peak is positioned at ~1050 cm^{-1}, which is attributed to the stretching vibration of C–O–H bonds of glycosidic structure in galactomannan polysaccharide sugars of coffee.[1, 2]

Fig. S4 also illustrates the molecular structure of two principal compounds present in the fresh coffee, which are galactomannan and lignin. The transformation, through heat treatment of fresh coffee at 450˚C (TC), leads to a considerable decrease in the peak intensities at 1050, 1700, and 3000 cm^{-1}. Subsequently, raising the temperature to 750˚C (Fe-750) leads to breakage of the chemical bonds and thus removal of the organic components. It is significant to note that the aromatic bonds, in lignin, and galactose chains, in galactomannan of the fresh coffee, can be responsible for generation of the fixed carbon after heat treatment.[3, 4]

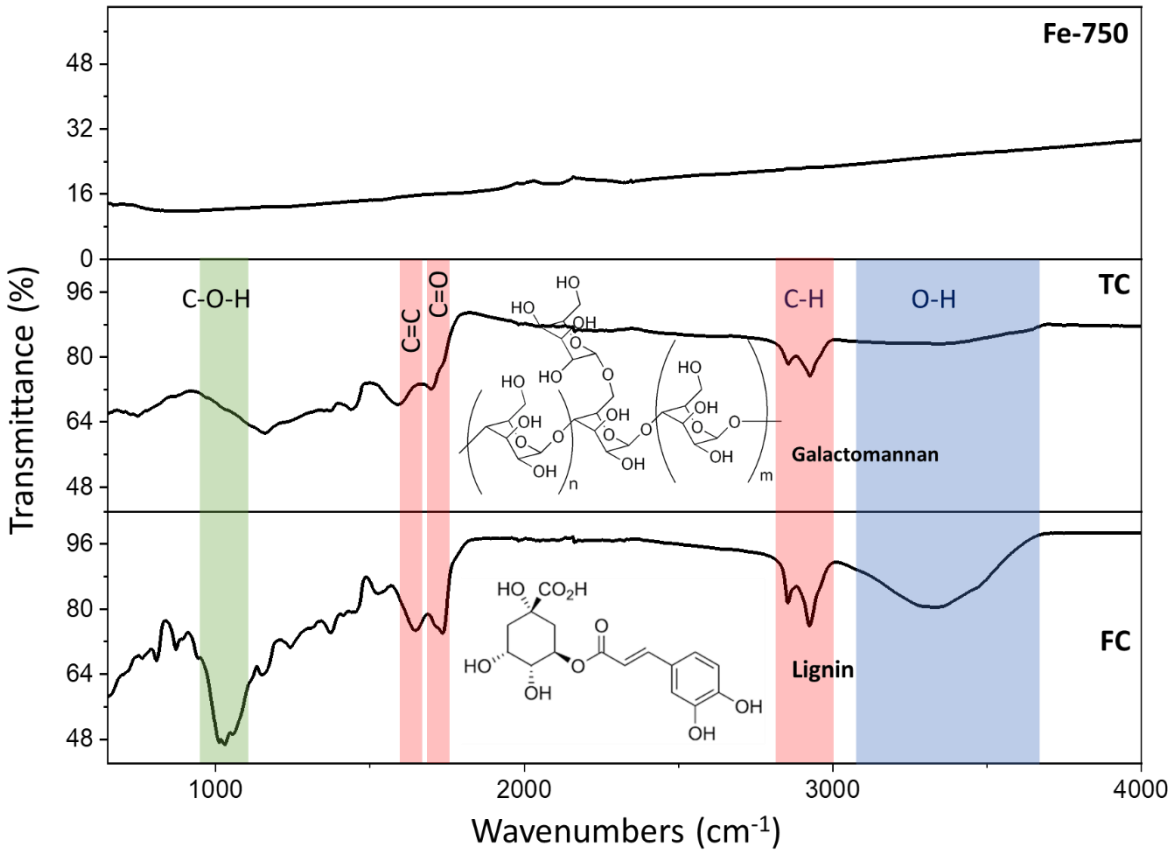

Fig. S4 FTIR spectra of fresh coffee (FC), transformed coffee (TC) by heat treatment at 450˚C, hybrid Fe-750 heat-treated at 750˚C.

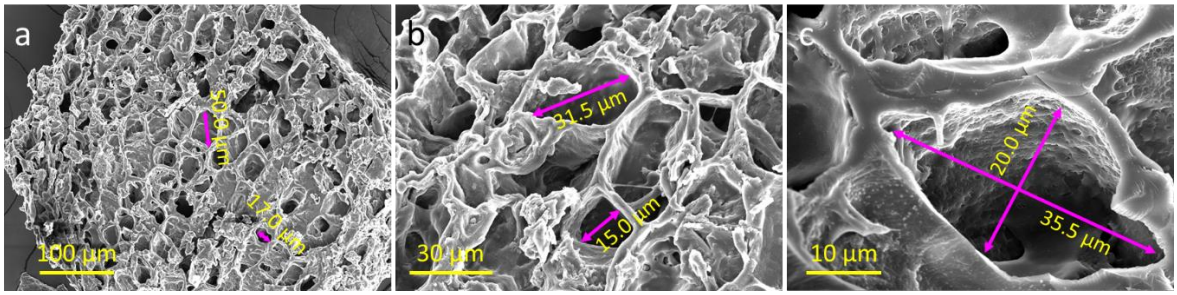

Fig. S5 FESEM images of MCS scaffold; the size of the macropores are measured and labelled in yellow.

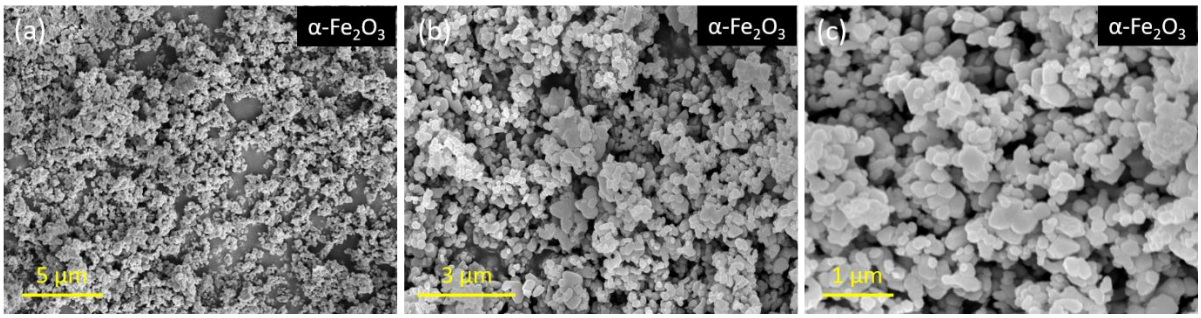

Fig. S6 FESEM images of iron oxide without direct interactions with MCS.

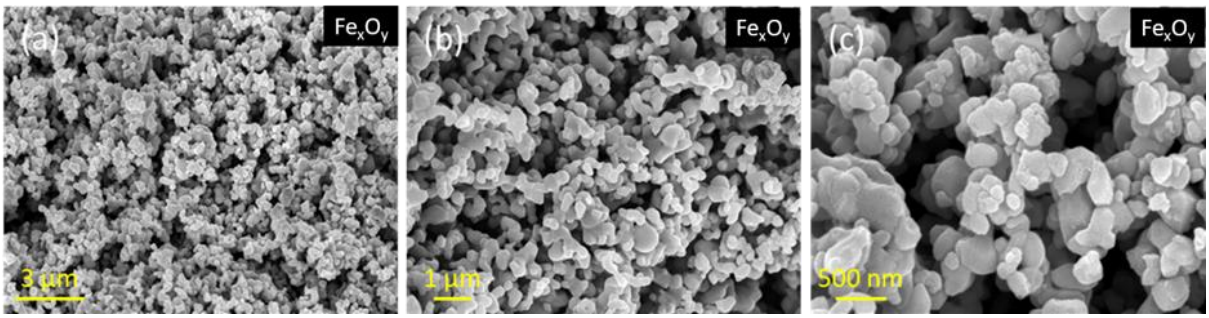

Fig. S7 FESEM images of Fe_xO_y integrated with nanoperforates of the MCS.

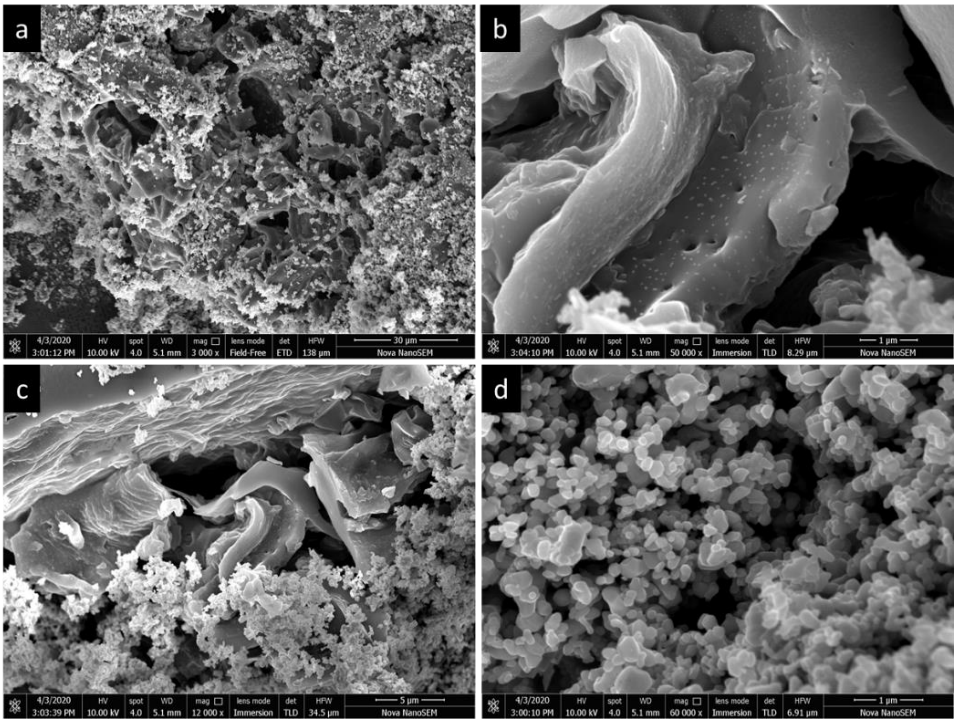

Fig. S8 FESEM images of Fe-750: Fe_xO_y integrated with nanoperforates of the MCS.

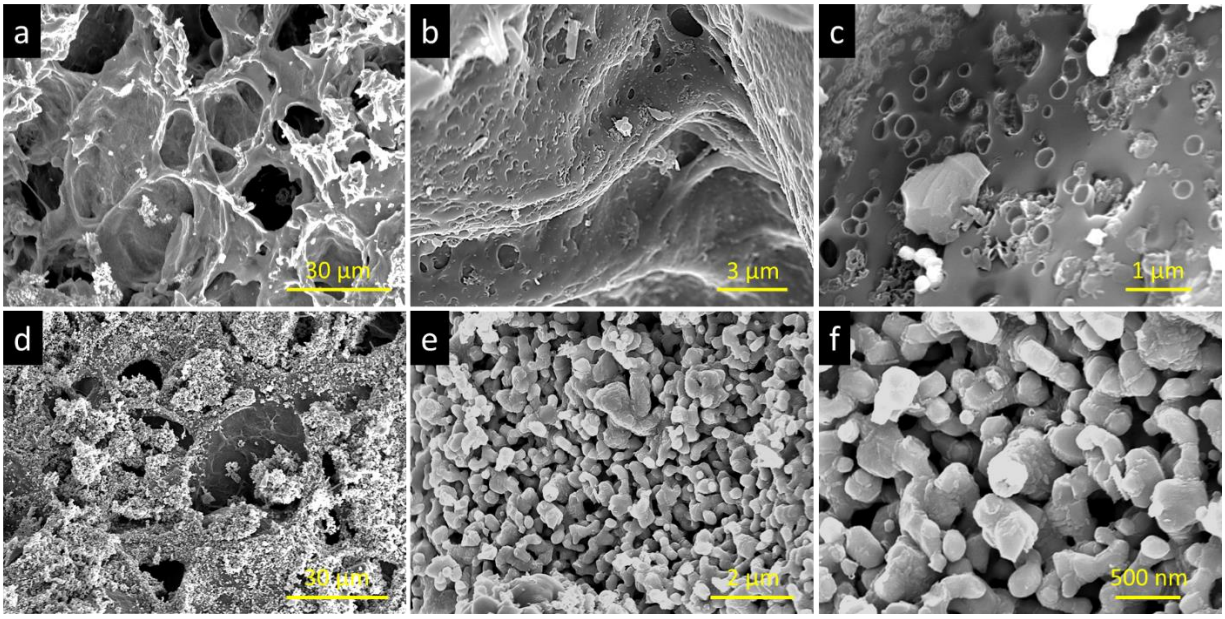

Fig. S9 FESEM images of Fe-950: Fe_xO_y integrated with nanoperforates of the MCS.

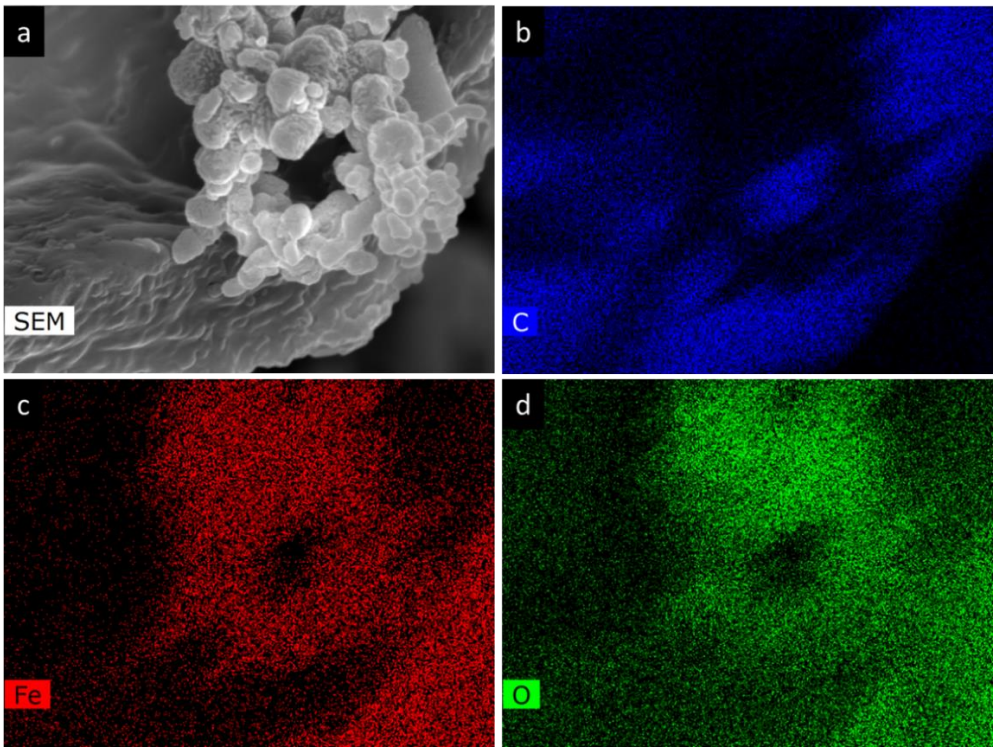

Fig. S10 EDS mapping of Fe-750, depicting elemental distributions of (b) Carbon, (c) Fe, and (d) O.

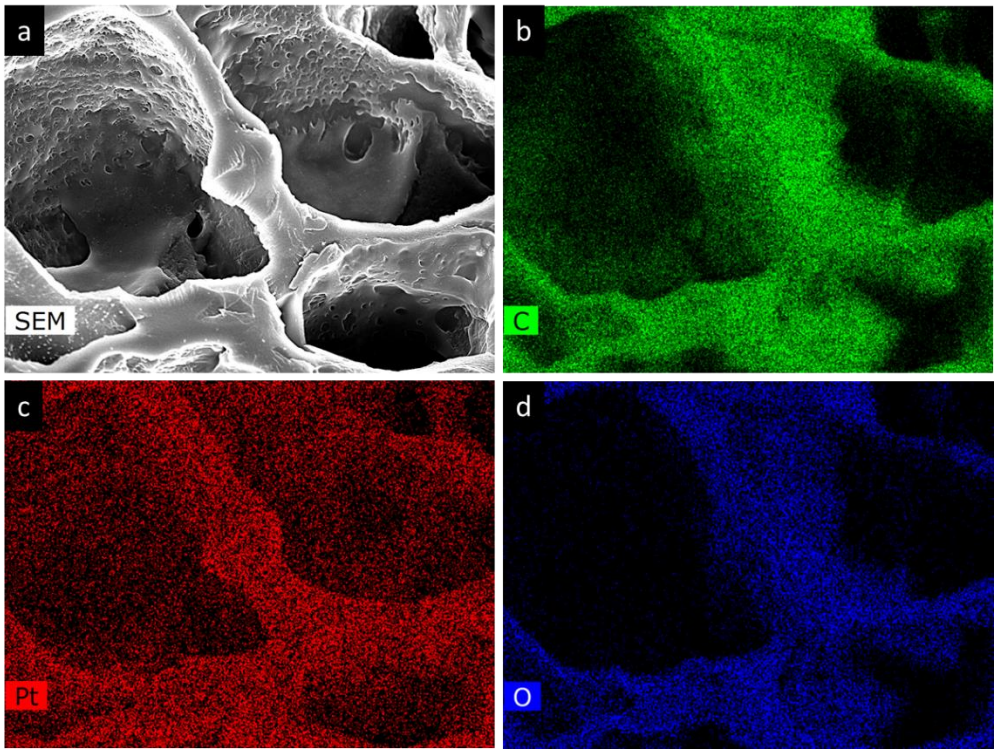

Fig. S11 EDS mapping of Fe-950 depicting elemental distributions of (b) Carbon, (c) Fe, and (d) O.

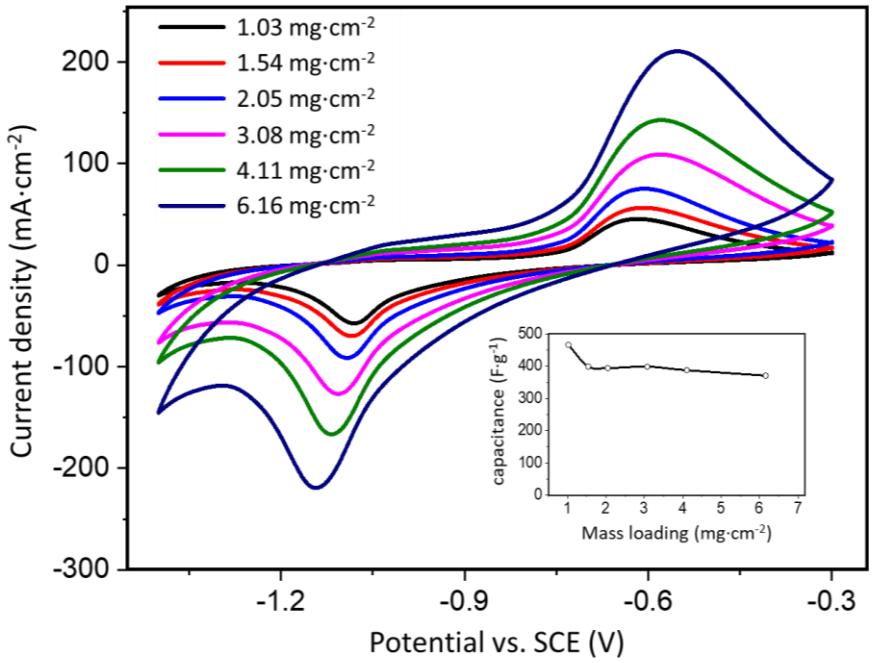

Fig. S12 Cyclic voltammograms for the hybrid MCS/Fe_xO_y (Fe-850) with variant mass loading between 1.03 and 6.16 mg·cm^{-2} at 100 mV.s^{-1} in 5M KOH. The inset shows the capacitance alterations as a function of the mass loading.

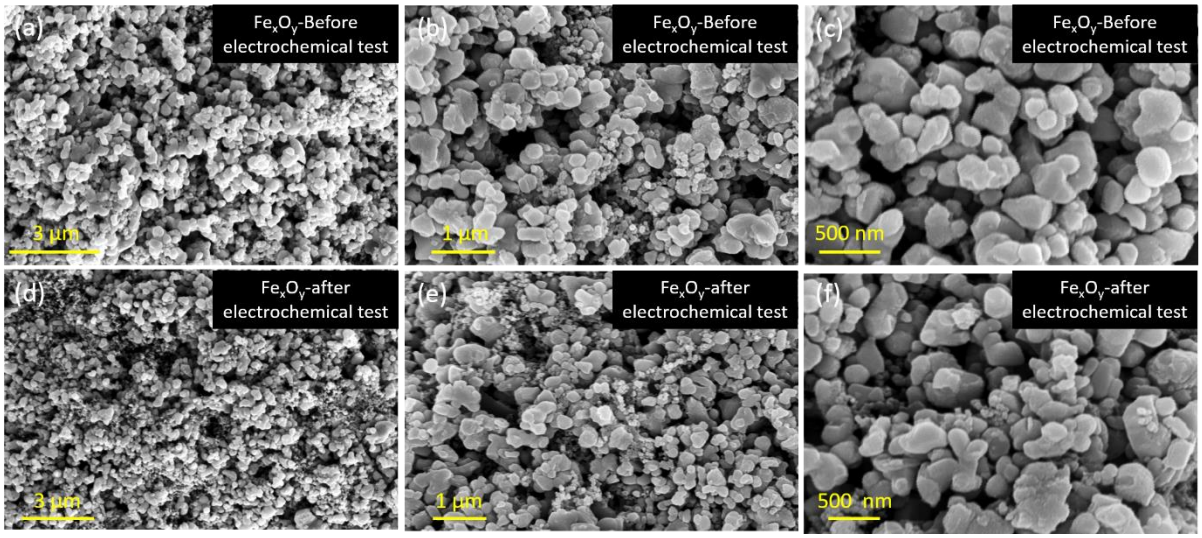

Fig. S13 FESEM images of hybrid MCS/Fe_xO_y (a-c) before and (d-f) after electrochemical tests. The smaller nanoparticles among the iron oxides are carbon black powders used to prepare required inks for the electrochemical tests.

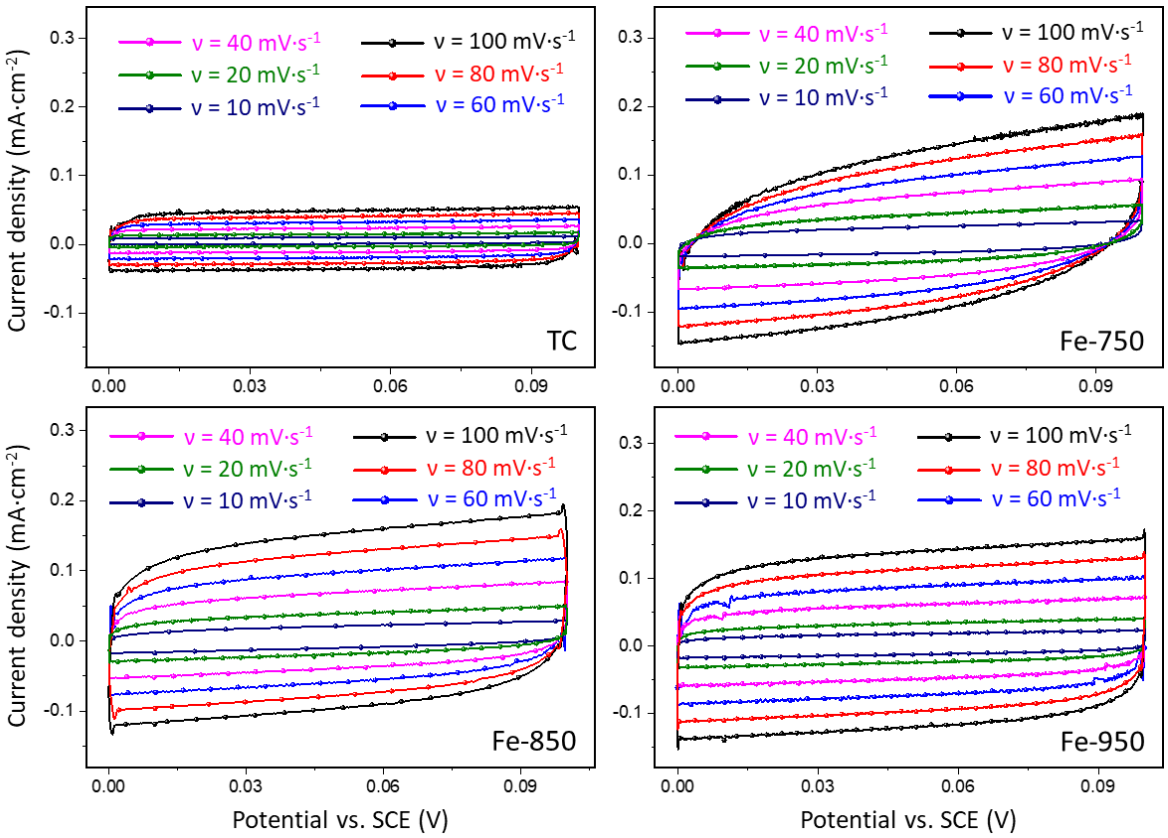

Fig. S14. Electrochemical surface area (ECSA) analysis of the TC, Fe-750, Fe-850, Fe-950, at scan rates ranging from 10-100 mV·s^{-1} in 5 M KOH.

Table S5 Selected performance table for single Fe_2O_3 and Fe_3O_4 phases as supercapacitor.

NO.	Fe_xO_y electrode	Synthesis method	Electrolyte	Potential range (V vs. X)	Specific Capacitance ($F\ g^{-1}$)	Cycles/ Retention (%)	SSA $m^2\ g^{-1}$	Ref
Fe_2O_3								
1	α-Fe_2O_3 NTs	Anodization	1 M Li_2SO_4	(-0.8) – (0) X = SCE	138 @ 1.3 $A\cdot g^{-1}$	500/ 89	-	5
2	Fe_2O_3 nanotube	-	1 M Na_2SO_4	(-1.0) – (0) X = SCE	92 @ 5 $mV\cdot s^{-1}$	3000/ 91	-	6
3	Fe_2O_3	Hydrothermal	0.5 M H_2SO_4	(-0.2) – (+1.0) X = Ag/AgCl	200 @ 1 $A\cdot g^{-1}$	2000/ 42	8	7
4	Fe_2O_3/ carbon cloth	Molten salt	6 M KOH	(-1.0) – (0) X = Hg/HgO	241 @ 2 $mV\cdot s^{-1}$	10,000/ 95	70	8
5	α-Fe_2O_3/ graphene	Hydrothermal	1 M Na_2SO_4	(-1.2) – (–0.2) X = Ag/AgCl	307 @ 3 $A\cdot g^{-1}$	2000/ 92	-	9
6	Fe_2O_3	Hummers (hydrothermal + freeze-drying	1 M KOH	(-1.1) – (–0.3) X = Hg/HgO	91 @ 50 $A\cdot g^{-1}$	70/ 51	-	10
7	Fe_2O_3/ graphene	Hydrothermal	1 M KOH	(-1.0) – (0) X = Ag/AgCl	114 @ 5 $A\cdot g^{-1}$	92/ 2000	-	11
8	Fe_2O_3/ carbon	Bottom-up assembly	1 M Na_2SO_3	(−1.0) – (−0.2) X = Ag/AgCl	235 @ 0.5 $A\cdot g^{-1}$	95/ 380	540	12
9	α-Fe_2O_3/ graphene	Hummers (hydrothermal + freeze-drying	1 M Na_2SO_4	(-1.0) – (0) X = Ag/AgCl	215 @ 2.5 $mV\cdot s^{-1}$	2000/ 89	-	11
10	α-Fe_2O_3/ Graphene	Hummers (hydrothermal + freeze-drying	1 M Na_2SO_4	(-1.0) – (0) X = Ag/AgCl	30 $F\cdot g^{-1}$ @ 2.5 $mV\cdot s^{-1}$	2000/ 92	-	11
11	α-Fe_2O_3/ rGO	Hydrothermal	-	(-1.2) – (–0.2) X = SCE	226 @ 1 $A\cdot g^{-1}$	-	-	13
12	Fe_2O_3 thin film	Ionic layer adsorption and reaction	1 M NaOH	(-0.6) – (+0.1) X = SCE	178 @ 5 $mV\cdot s^{-1}$	-	-	14
Fe_3O_4								
No.	**Fe_xO_y electrode**	**Synthesis method**	**Electrolyte**	**Potential range (V vs. X)**	**Specific capacitance ($F\ g^{-1}$)**	**Cycle/ Retention (%)**	**SSA $m^2\ g^{-1}$**	**Ref**

13	Fe_3O_4/ Graphene	Wet chemistry following by heat treatment	1 M KOH	(-1.0) – (0.0) X = Hg/HgO	368 @ 1 A g^{-1}	1000/ 66	346	15
14	Fe_3O_4/ rGO	Hydrothermal	1 M KOH	(-1.0) – (0.0) X = Ag/AgCl	241 @ 1 A g^{-1}	1000/ 79	151	16
15	Fe_3O_4/ rGO	electrostatic assembly	6 M KOH	(0.0) – (1.4) X = SCE	193 @ 0.3 A g^{-1}	1000/ 90	173	17
16	Fe_3O_4 NPs	Sol-gel	3M KOH	(-0.9) – (-0.1) X = SCE	185 @ 1 A g^{-1}	200/ 66	-	18
17	Fe_3O_4 nanorod	Hydrothermal	1M Na_2SO_3	(-1.0) – (0.0) X = SCE	208 @ 0.5 A g^{-1}	500/ 73	-	19
18	Fe_3O_4	Chemical	6 M KOH	(-1.0) – (+0.4) X = Hg/HgO	160 @ 1 A·g^{-1}	1000/ 86	-	20
19	Fe_3O_4/Au	Chemical	6 M KOH	(-1.0) – (+0.4) X = Hg/HgO	464 @ 1 A·g^{-1}	1000/ 72	-	20
20	Fe_3O_4 film	Hydrothermal	1 M Na_2SO_3	(-1.0) – (0.1) X = SCE	118 6 mA	500/ 88	-	21
21	Fe_3O_4 film	Hydrothermal/ spray deposition	0.1 M Na_2SO_3	(-1.2) – (0.0) X = SCE	106 @ 0.1 mA·cm^{-2}	500/ 80	48	22
22	Carbon QD decorated Fe_3O_4	Solvothermal/ ultrasonication	1 M Na_2SO_3	(0.0) – (1.0) X = SCE	208 @ 1 A·g^{-1}	200/ 54	-	23
23	Fe_3O_4/ N-doped carbon NWs	Capping agent-assisted wet chemistry, annealing	3 M KOH	(-1.0) –(-0.3) X = Hg/HgO	541 @ 1 A·g^{-1}	5000/ 68	-	24
24	Fe_3O_4/ FeOOH	Spray deposition	1 M Na_2SO_3	(-1.0) – (-0.0) X = SCE	300 @ 2 mV·s^{-1}	100/ 78	-	25
25	Fe_3O_4 nanoflake	Hydrothermal	2 M KOH	(-1.0) – (-0.0) X = SCE	379 @ 2 A·g^{-1}	2000/ 99	-	26

References:

1. L. Hao, N. Wang, C. Wang and G. Li, *Chemosphere*, 2018, **202**, 768-776.
2. L. F. Ballesteros, J. A. Teixeira and S. I. Mussatto, *Food and Bioprocess Technology*, 2014, **7**, 3493-3503.
3. W. Qu and X. Bai, *Journal of Applied Polymer Science*, 2020, **137**, 48843.
4. J. Verbančič, J. E. Lunn, M. Stitt and S. Persson, *Molecular Plant*, 2018, **11**, 75-94.
5. K. Xie, J. Li, Y. Lai, W. Lu, Z. a. Zhang, Y. Liu, L. Zhou and H. Huang, *Electrochemistry Communications*, 2011, **13**, 657-660.
6. G. S. Gund, D. P. Dubal, N. R. Chodankar, J. Y. Cho, P. Gomez-Romero, C. Park and C. D. Lokhande, *Scientific Reports*, 2015, **5**, 12454.
7. S. Rudra, R. Chakraborty, P. K. Maji, S. Koley, A. K. Nayak, D. Paul and M. Pradhan, *Electrochimica Acta*, 2019, **324**, 134865.
8. Y.-J. Gu, W. Wen, S. Zheng and J.-M. Wu, *Materials Chemistry Frontiers*, 2020, **4**, 2744-2753.
9. S. Yang, X. Song, P. Zhang, J. Sun and L. Gao, *Small*, 2014, **10**, 2270-2279.
10. H. Wang, Z. Xu, H. Yi, H. Wei, Z. Guo and X. Wang, *Nano Energy*, 2014, **7**, 86-96.
11. K. K. Lee, S. Deng, H. M. Fan, S. Mhaisalkar, H. R. Tan, E. S. Tok, K. P. Loh, W. S. Chin and C. H. Sow, *Nanoscale*, 2012, **4**, 2958-2961.
12. Y. Lin, X. Wang, G. Qian and J. J. Watkins, *Chemistry of Materials*, 2014, **26**, 2128-2137.
13. Z. Wang, C. Ma, H. Wang, Z. Liu and Z. Hao, *Journal of Alloys and Compounds*, 2013, **552**, 486-491.
14. P. M. Kulal, D. P. Dubal, C. D. Lokhande and V. J. Fulari, *Journal of Alloys and Compounds*, 2011, **509**, 2567-2571.
15. M. Liu and J. Sun, *Journal of Materials Chemistry A*, 2014, **2**, 12068-12074.
16. L. Li, P. Gao, S. Gai, F. He, Y. Chen, M. Zhang and P. Yang, *Electrochimica Acta*, 2016, **190**, 566-573.
17. F. Yan, J. Ding, Y. Liu, Z. Wang, Q. Cai and J. Zhang, *Synthetic Metals*, 2015, **209**, 473-479.
18. E. Mitchell, R. K. Gupta, K. Mensah-Darkwa, D. Kumar, K. Ramasamy, B. K. Gupta and P. Kahol, *New Journal of Chemistry*, 2014, **38**, 4344-4350.
19. J. Liu, S. Liu, S. Zhuang, X. Wang and F. Tu, *Ionics*, 2013, **19**, 1255-1261.
20. S. Liu, S. Guo, S. Sun and X.-Z. You, *Nanoscale*, 2015, **7**, 4890-4893.
21. J. Chen, K. Huang and S. Liu, *Electrochimica Acta*, 2009, **55**, 1-5.
22. X. Zhao, C. Johnston, A. Crossley and P. S. Grant, *Journal of Materials Chemistry*, 2010, **20**, 7637-7644.
23. K. Bhattacharya and P. Deb, *Dalton Transactions*, 2015, **44**, 9221-9229.
24. J. Chen, Q. Chen, J. Xu and C.-P. Wong, *RSC Advances*, 2017, **7**, 48039-48046.
25. L. O'Neill, C. Johnston and P. S. Grant, *Journal of Power Sources*, 2015, **274**, 907-915.
26. F. Li, H. Chen, X. Y. Liu, S. J. Zhu, J. Q. Jia, C. H. Xu, F. Dong, Z. Q. Wen and Y. X. Zhang, *Journal of Materials Chemistry A*, 2016, **4**, 2096-2104.